HYDROLOGICAL PROCESSES
Hydrol. Process. **17**, 3465–3483 (2003)
Published online in Wiley InterScience (www.interscience.wiley.com). DOI: 10.1002/hyp.1394

Ice-cover variability on shallow lakes at high latitudes: model simulations and observations

Claude R. Duguay,[1]* Greg M. Flato,[2] Martin O. Jeffries,[1] Patrick Ménard,[3] Kim Morris[1] and Wayne R. Rouse[4]

[1] *Geophysical Institute, University of Alaska Fairbanks, Fairbanks, AK 99775-7320, USA*
[2] *Canadian Centre for Climate Modelling and Analysis, Atmospheric Environment Service, P.O. Box 1700, Victoria, British Columbia V8W 2Y2, Canada*
[3] *Laboratoire de télédétection et de modélisation des environnements froids, Centre d'études nordiques et Département de géographie, Université Laval, Cité universitaire, Sainte-Foy, Québec G1K 7P4, Canada*
[4] *School of Geography and Geology, McMaster University, Hamilton, Ontario L8S 4K1, Canada*

Abstract:

A one-dimensional thermodynamic model for simulating lake-ice phenology is presented and evaluated. The model can be driven with observed daily or hourly atmospheric forcing of air temperature, relative humidity, wind speed, cloud amount and snowfall. In addition to computing the energy balance components, key model output includes the temperature profile at an arbitrary number of levels within the ice/snow (or the water temperature if there is no ice) and ice thickness (clear ice and snow-ice) on a daily basis, as well as freeze-up and break-up dates. The lake-ice model is used to simulate ice-growth processes on shallow lakes in arctic, sub-arctic, and high-boreal forest environments. Model output is compared with field and remote sensing observations gathered over several ice seasons. Simulated ice thickness, including snow-ice formation, compares favourably with field measurements. Ice-on and ice-off dates are also well simulated when compared with field and satellite observations, with a mean absolute difference of 2 days. Model simulations and observations illustrate the key role that snow cover plays on the seasonal evolution of ice thickness and the timing of spring break-up. It is also shown that lake morphometry, depth in particular, is a determinant of ice-off dates for shallow lakes at high latitudes. Copyright © 2003 John Wiley & Sons, Ltd.

KEY WORDS modelling; lake ice; snow; shallow lakes; tundra; forest

INTRODUCTION

One of the most obvious manifestations of the hydrological system at work in high-latitude regions is the vast number of lakes. Estimates of the areal coverage of lakes in the arctic and sub-arctic regions of the Northern Hemisphere range from 15 to 40%, depending on location, which places them as a major component of the terrestrial landscape. These lakes range from those that are little more than 1 m deep, but often several km^2 in surface area, to those that are very deep and very large (e.g. Great Slave Lake and Great Bear Lake, Northwest Territories, Canada). The most important characteristic of lakes of all sizes is their ability to store heat. Shallow lakes have thermal turnover rates (heat gains = heat losses) in the order of a week (Stewart and Rouse, 1977), whereas for the large deep ones, the turnover is in the order of 6 to 8 months (Schertzer, 1997; Blanken *et al.*, 2000).

Lakes are very sensitive to climate change because they are often ice-covered during the high sun period around the summer solstice. Thus, climate change in the form of global warming has the potential to greatly enhance the energy and moisture exchange over lakes by stimulating earlier thaw and increasing the absorption

* Correspondence to: Claude R. Duguay, Geophysical Institute, University of Alaska Fairbanks, Fairbanks, AK 99775–7320, USA.
E-mail: claude.duguay@gi.alaska.edu

Received 5 November 2001
Accepted 15 May 2003

Copyright © 2003 John Wiley & Sons, Ltd.

of solar radiation. Also, later freeze-back dates means that more evaporative moisture will be transferred to the atmosphere during early winter. Because lakes are such a major component of most northern atmospheric and hydrologic systems, the ability to model their annual energy and water budgets is critical to our ability to forecast high latitude weather, climate and river flow patterns.

The decay and eventual break-up of lake ice also represents a temporally and spatially integrated response to the weather conditions prevailing during a period of several weeks in late winter to early spring (Livingstone, 1997). Long series of lake-ice observations can serve as a proxy climate record, and the monitoring of freeze-up and break-up trends has been shown to provide a convenient integrated and seasonally specific index of climatic perturbations. For example, freeze and break-up dates change by approximately 4–7 days for every degree (Celsius) change in air temperature (O'Neill *et al.*, 2001). Small (shallow) lakes, which are conspicuous features of circumpolar regions, are well suited for investigating the impact of climatic variability and climate change on ice cover because the effects of heat storage and circulation are reduced; larger lakes provide an integrated response to regional change involving several related elements (e.g. temperature, precipitation, runoff). On the North Slope of Alaska, for example, there are thousands of shallow lakes that typically cover 20% of the land in most places, and as much as 40% near the coast (Sellmann *et al.*, 1975a). Similar lake-dominated areas can be found on the coastal plains of East Siberia (Grosswald *et al.*, 1999), the Hudson Bay Lowlands (Duguay *et al.*, 1999), the Old Crow Flats of the Yukon Territory (Lauriol *et al.*, 2002), and the delta of the Mackenzie River in the Northwest Territories. The lakes are actually ice-free for only a short period, 6–16 weeks, each year, and because they are shallow, may freeze to the bottom (Sellmann *et al.*, 1975b; Jeffries *et al.*, 1994, 1996; Duguay and Lafleur, 2003).

In recent years, several physically based models have been developed to simulate lake-ice growth and examine the sensitivity of ice phenology to climate change (e.g. Heron and Woo, 1994; Liston and Hall, 1995, Vavrus *et al.*, 1996; Stefan and Fang, 1997). The one-dimensional thermodynamic ice model used here and referred to as CLIMo (Canadian Lake Ice Model), is similar to some of these models. However, it also presents some notable differences, particularly in the parameterization of snow conductivity and surface albedo. In this paper, we describe the model and present results of simulations carried out on shallow lakes in three distinct high-latitude environments (arctic, sub-arctic, and high-boreal forest). Whereas previous investigations have primarily concentrated on comparing model output (e.g. total ice thickness and/or ice-on/ice-off dates) with field observations over a limited number of lakes and/or a limited number of environments, this study includes comparison with both *in situ* and remote-sensing observations in regions experiencing significantly different snow regimes. Detailed field observations at ponds in the high-boreal forest region allow us to evaluate the model's ability to simulate snow-ice formation. The remote-sensing observations allow us to monitor the disappearance of ice cover at the regional scale, thereby enabling us to identify components of the model that may require future improvements.

MODEL DESCRIPTION

General description

The Canadian Lake Ice Model is an adaptation of the one-dimensional thermodynamic sea-ice model of Flato and Brown (1996). The model is based on the one-dimensional unsteady heat conduction equation, with penetrating solar radiation, presented by Maykut and Untersteiner (1971), i.e.

$$\rho C_p \frac{\partial T}{\partial t} = \frac{\partial}{\partial z} k \frac{\partial T}{\partial z} + F_{sw} I_o (1-\alpha) K e^{-Kz} \tag{1}$$

where $T(z, t)$ is the temperature within the ice or snow, t is time and z is depth measured positive downward from the upper surface (Figure 1). Briefly, the model solves Equation (1) by using an implicit-in-time, centred-in-space, finite-difference numerical scheme that may have an arbitrary number of layers in both the ice and snow portions of the slab and is unconditionally stable.

Copyright © 2003 John Wiley & Sons, Ltd.

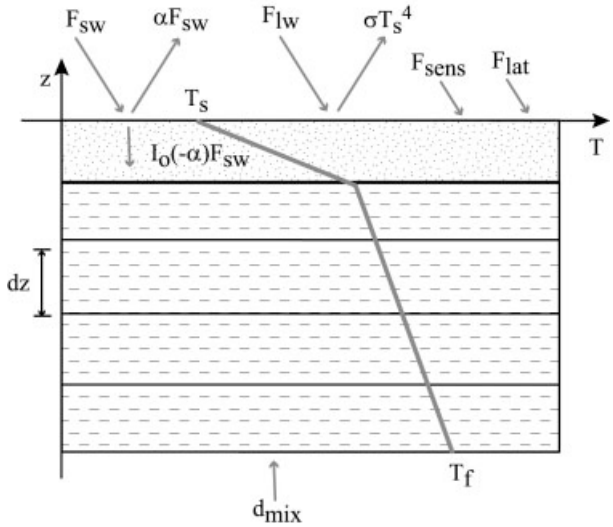

Figure 1. Schematic illustration of the lake ice model during winter. The layers with dashed lines represent ice and the layer with dots is snow. The heavy grey line indicates the temperature profile, which is computed using a finite-difference representation of the heat conservation Equation (1). The grey arrows along the top of the surface indicate the components of the surface heat budget included in the model. See Equations (1) through to (13) for details on each parameter

Equation (1) is subject to the following boundary conditions: at the ice underside

$$T(h, t) = T_{\mathrm{f}} \tag{2}$$

where h is the total thickness of the ice plus snow and T_{f} is the freezing temperature of fresh water (i.e. the ice underside is always at the freezing point). At the upper surface

$$\begin{aligned} T(0, t) &= T_{\mathrm{m}} \qquad F_0 > 0, \hat{T}(0) \geq T_{\mathrm{m}} \\ k \left.\frac{\partial T}{\partial z}\right|_{z=0} &= F_0 \qquad \text{otherwise} \end{aligned} \tag{3}$$

where T_{m} is the melting temperature at the surface, F_0 is the net heat flux absorbed at the surface and $\hat{T}$ is the estimated temperature prior to solving Equation (1). Equation (3) states that the upper surface boundary condition is the net surface heat flux, obtained from the surface energy budget calculation described later (Equation 13), except when the surface is melting. When melt is occurring at the upper surface, the boundary condition is that temperature is fixed at the melting point for fresh water and the heat flux offsets the latent heat of fusion of melting ice or snow. A generalized Crack–Nicholson, finite-difference numerical scheme, is used to solve Equations (1)–(3) (see Flato and Brown (1996) for details).

In order to permit an annual cycle in which the ice melts away completely in summer, the model also includes a fixed-depth mixed layer. When ice is present, the mixed layer is fixed at the freezing point, and when ice is absent, the mixed layer temperature is computed from the surface energy budget, namely

$$\rho_{\mathrm{w}} C_{\mathrm{pw}} d_{\mathrm{mix}} \frac{\partial T_{\mathrm{mix}}}{\partial t} = F_0 + F_{\mathrm{sw}} I_0 (1 - \alpha) \tag{4}$$

where T_{mix} is the mixed layer temperature and d_{mix} is the effective mixed layer depth (a measure of the heat storage available in the lake). The water column of shallow lakes is typically well-mixed (and isothermal) from top to bottom during the ice-free period, so that d_{mix} provides a good approximation of the effect of lake depth leading to autumn freeze-up.

Copyright © 2003 John Wiley & Sons, Ltd.

Growth and melt at the ice underside are computed from the difference between the conductive heat flux into the ice and the heat flux out of the upper surface of the mixed layer; thus

$$\left.\frac{\partial h_{\mathrm{i}}}{\partial t}\right|_{z=h} = \left(k\left.\frac{\partial T}{\partial z}\right|_{z=h} - \int_{h}^{\infty} F_{\mathrm{sw}} I_0 (1-\alpha) K \mathrm{e}^{-Kz} \mathrm{d}z\right)\frac{1}{L_{\mathrm{fi}}} \tag{5}$$

where h_{i} is the ice thickness. The last term of Equation (5) is the shortwave radiation that penetrates through the bottom of the ice slab, and is assumed to be absorbed in the mixed layer and returned to the ice underside in order to keep the temperature of the mixed layer at the freezing point. The mixed layer also may be subjected to heat flux from the lake sediments. Variations in heat exchanges between the water column and bottom sediments over the full annual cycle, however, are not explicitly simulated. Instead, a fixed (constant) heat flux from the lake bottom is used. We recognize this to be a simplification of heat exchanges for small, shallow, lakes that will need to be addressed, substantiated by quality field observations, in a future version of the model.

Melt at the upper surface is computed from the difference between the conductive flux and the net surface flux; any snow is melted first and the remaining heat is used to melt ice, i.e.

$$\left.\frac{\partial h_{\mathrm{s}}}{\partial t}\right|_{z=0} = \left(F_0 - k\left.\frac{\partial T}{\partial z}\right|_{z=0}\right)\frac{1}{L_{\mathrm{fs}}} \qquad h_{\mathrm{s}} > 0 \tag{6}$$

$$\left.\frac{\partial h_{\mathrm{i}}}{\partial t}\right|_{z=0} = \left(F_0 - k\left.\frac{\partial T}{\partial z}\right|_{z=0}\right)\frac{1}{L_{\mathrm{fi}}} \qquad h_{\mathrm{s}} = 0 \tag{7}$$

where h_{s} is the snow depth. Two additional mechanisms exist to change the ice thickness: (i) if there is sufficient snow to depress the ice surface below the water level, the flooded snow (slush) is converted into snow-ice, and (ii) if, after advancing Equation (1) by one time-step, the temperature at any level is greater than T_{m}, it is reset to T_{m} and the corresponding heat is used to melt ice. In order to conserve energy, the latent heat released by freezing porewater when converting slush into snow ice is returned to the ice slab as a source of heat at the ice surface. In situations where the liberated heat raises the ice temperature above freezing, the melt temperature constraint just described will melt a corresponding amount of ice. Ice surface temperature in winter is generally low enough to accommodate this latent heat release.

Parameterizations

Many parameterizations used in this model follow closely those of Ebert and Curry (1993). The two parameterizations that are most unique to CLIMo are those of snow conductivity (and heat capacity) and surface albedo.

The parameterization of snow conductivity and heat capacity is

$$k(z) = c_1\rho_{\mathrm{s}}^2 + c_2 2^{[T(z)-c_3]c_4} \qquad z < h_{\mathrm{s}} \tag{8}$$

$$\rho C_{\mathrm{p}}(z) = \rho_{\mathrm{s}}[c_5 + c_6 T(z)] \qquad z < h_{\mathrm{s}} \tag{9}$$

where $z \geq h_{\mathrm{s}}$, $k(z)$ and $\rho\ C_{\mathrm{p}}(z)$ are the conductivity and heat capacity of freshwater ice ($k_{\mathrm{if}} = 2{\cdot}034$ W m^{-1} K^{-1} and $\rho_{\mathrm{i}} C_{\mathrm{pi}} = 1{\cdot}883 \times 10^{-6}$ J m^{-3} K^{-1}).

The parameterization of surface albedo reflects the strong dependence on surface type (ice, snow, or open water), surface temperature (melting versus subfreezing), and ice thickness. The latter acts as a proxy for time in the melt season and allows a parameterization that attempts to capture the evolution of melt ponds on the surface. The cold ice albedo parameterization is from Maykut (1982), whereas the melting ice parameterization

Copyright © 2003 John Wiley & Sons, Ltd.

is based on the Arctic lake-ice observations of Heron and Woo (1994). The parameterization is summarized as follows

$$\alpha = \begin{cases} \alpha_{\mathrm{ow}} & h_{\mathrm{i}} < h_{\mathrm{min}} \\ \min[\alpha_{\mathrm{s}}, \alpha_{\mathrm{i}} + h(\alpha_{\mathrm{s}} - \alpha_{\mathrm{i}})/c_7] & h_{\mathrm{i}} \geq h_{\mathrm{min}} \quad h_{\mathrm{i}} \leq c_7 \\ \alpha_{\mathrm{s}} & h_{\mathrm{i}} \geq h_{\mathrm{min}} \quad h_{\mathrm{s}} > c_7 \end{cases} \tag{10}$$

$$\alpha_{\mathrm{i}} = \begin{cases} \max(\alpha_{\mathrm{ow}}, c_8 h_{\mathrm{i}}^{0\cdot 28} + 0\cdot 08) & T(0,t) < T_{\mathrm{m}} \\ \min(\alpha_{\mathrm{mi}}, c_9 h_{\mathrm{i}}^2 + \alpha_{\mathrm{ow}}) & T(0,t) = T_{\mathrm{m}} \end{cases} \tag{11}$$

$$\alpha_{\mathrm{s}} = \begin{cases} 0\cdot 75 & T(0,t) < T_{\mathrm{m}} \\ 0\cdot 65 & T(0,t) = T_{\mathrm{m}} \end{cases} \tag{12}$$

Surface energy budget

The surface energy budget is

$$F_0 = F_{\mathrm{lw}} - \varepsilon\sigma T_{\mathrm{s}}^4(0,t) + (1-\alpha)(1-I_0)F_{\mathrm{sw}} + F_{\mathrm{lat}} + F_{\mathrm{sens}} \tag{13}$$

where F_{lw} is the downward longwave radiative flux and F_{lat} and F_{sens} are the downward latent and sensible heat fluxes, respectively. The downward longwave flux is computed using the formula of Maykut and Church (1973), whereas the downward shortwave flux is computed using the equation of Shine (1984). Sensible and latent heat fluxes are computed as described in Ebert and Curry (1993), but with the atmospheric turbulence parameter ($b' = 4\cdot 7$) as given by Louis (1979).

All of the terms in Equation (13), except the downward longwave flux, depend explicitly or implicitly on surface temperature. Therefore a Newton–Raphson iterative scheme is used to find the surface temperature $T(0,t)$ that simultaneously satisfies Equations (1)–(3) and (13). Since the surface temperature evolves relatively slowly, the Newton–Raphson scheme generally converges in two or three iterations (where convergence is defined by a surface temperature change between consecutive iterations of less than 0·01 K).

Atmospheric forcing and model output

The model can be forced with daily mean or hourly values of air temperature, relative humidity, cloud amount, wind speed and snowfall. When snow density measurements are available, these can be read as an input, whether as a constant, mean winter value or as a daily variable, linearly interpolated from snow course observations (MSC, 2000; Ménard *et al.*, 2002). The downward radiative terms either can be read directly, in situations where tower measurements are available, or computed using bulk formulae as described in the previous section. In addition to the energy balance components, key model output includes snow depth, the temperature profile at an arbitrary (specified) number of levels within the ice/snow (or the water temperature if there is no ice) and ice thickness (clear ice and snow ice) on a daily basis, as well as freeze-up/break-up dates and end-of-season clear ice, snow ice and total ice thickness.

MODEL SIMULATIONS

Simulations were carried out on shallow lakes in three study areas: Barrow and Poker Flat Research Range (near Fairbanks), Alaska, and Churchill, Manitoba (Figure 2). These areas are representative of arctic (Barrow), sub-arctic (Churchill), and high-boreal forest (Poker Flat) environments. Temperature and snow accumulation regimes differ significantly between these regions. Snow depth, in particular, is different not only between but also within the study areas. This is particularly true of the Barrow and Churchill study areas where snow depth can be very thin and dense to non-existent on some lakes or lake sections. In the Poker Flat study area, on the other hand, the snow cover is relatively undistributed by wind and accumulates to a depth conducive

Copyright © 2003 John Wiley & Sons, Ltd.

Figure 2. Location of Barrow, Poker Flat (Fairbanks) and Churchill study areas

to the formation of snow-ice. These contrasting environments permit a more rigorous evaluation of the model than accomplished in previous studies.

All simulations were carried out using a daily time-step and an effective mixed layer depth of 2 m, a value close to the mean depth of the lakes and ponds of this investigation. For model testing, both long-term and individual ice-season comparisons were made against field and remote sensing observations. Measured precipitation data were not used for the simulations, as the model does not include details such as redistribution of snow by wind and because of the difficulty in accurately measuring snowfall, which frequently occurs as trace amounts (Metcalfe and Goodison, 1993). As a result, the precipitation problem was instead prescribed based on snow depth measurements made at the nearby weather stations. To evaluate the effect of uncertainty in snowfall several simulations are conducted with snowfall ranging from 0 to 100% of the value inferred from snow depth observations. As shown in Figure 3, snow accumulation can vary substantially between lakes and, to a lesser extent, on a given lake within a study area as a function of exposure to wind.

Barrow

The lakes investigated at Barrow, north-west Alaska, are located on the North Slope on tundra close to sea-level within 10 km of the coast (Table I). They are situated on tundra close to sea-level. The actual depth is known for only a few lakes. However, results of a study by Jeffries *et al*. (1996) using a numerical ice-growth model and spaceborne radar imagery suggest that, in the Barrow region, 23% of the lakes may be deeper than 2·2 m, 10% between 1·5 m and 2·2 m, 60% between 1·4 and 1·5 m, and 7% less than 1·4 m deep.

Barrow has a mean annual temperature of −12·5 C, mean annual snowfall of 71 cm, and mean annual wind speed of 19·1 km h^{-1}. Meteorological data from the National Weather Service (NWS) station at Barrow were used as input for simulations of the 1991–92 ice season. Based on field measurements made in winters 1991–1992, 1995–1996 and 1996–1997 in this region, Zhang and Jeffries (2000) indicate that the ratio between average snow depth measured over lake ice and snow depth measured at the Barrow NWS station

Table I. Location and dimensions of Barrow lakes

Lake	Latitude (N)	Longitude (W)	Length (km)	Width (km)
Emaiksoun Lake	71·23	156·23	2·5	1·0
Emikpuk Lake	71·33	156·65	1·1	0·6
Ikroavik Lake	71·24	156·65	4·1	1·7

Copyright © 2003 John Wiley & Sons, Ltd.

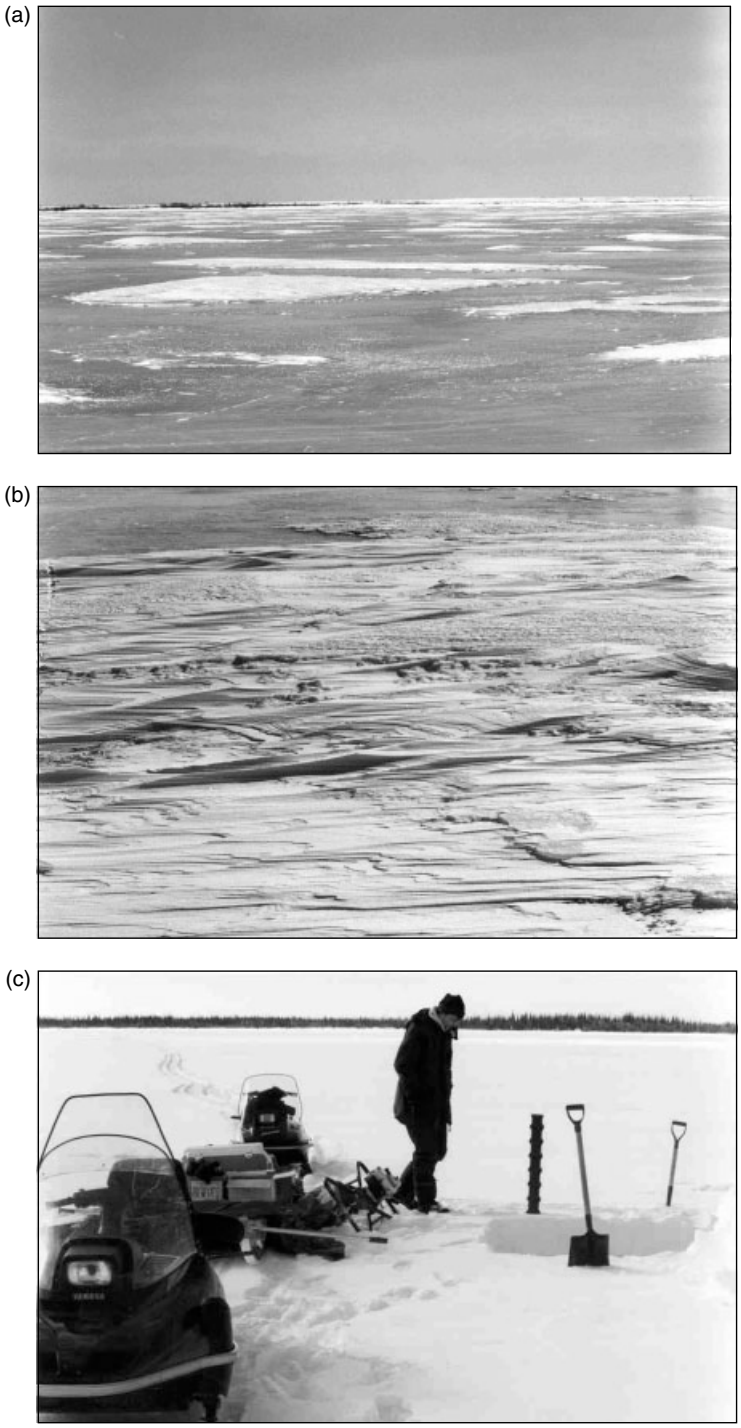

Figure 3. Photographs taken in late March 1998 in the Churchill study area showing examples of snow cover distribution on lakes in: (a) tundra zone (mostly bare patches of ice); (b) forest-tundra transition zone (snow drifts with bare patch of ice in upper left corner); and (c) open forest zone (relatively homogeneous and deep cover)

Copyright © 2003 John Wiley & Sons, Ltd.

(or snow cover fraction) ranges from 0·43 to 0·67, with an average of 0·52 (or 52%). However, this value is likely to vary temporally (during the course of winter) and spatially as snow can be more or less redistributed on some lakes. For example, snow depths measured at the Barrow NWS station varied between 31 cm and 25 cm from 19 to 29 April 1992. Jeffries *et al*. (1994) report that snow depth over lake-ice covers ranged from 0 and 8 cm during the same period. Therefore, given the wide variations in snow cover fraction, we opted to conduct several simulations in which snow depth was varied from 0% (no snow) to 100% (corresponding to the amount of snow measured at NWS station), with increments of 25%. An average snow density of 350 kg m^{-3} was used in model runs; a density value observed on lake-ice covers in the Barrow area (Jeffries *et al*., 1999).

The ERS-1 images acquired over the North Slope of Alaska during the spring thaw of 1992 were used for validating the simulated ice-off date, and ice thickness was compared against measurements made on some lakes in the study area between 19 and 29 April 1992 (Jeffries *et al*., 1994).

Churchill

The Churchill study area is located on the west coast of Hudson Bay (58 45′N, 94 04′W). It is in the physiographic region of the Hudson Bay Lowlands and lies near the southern limit of continuous permafrost and the northern treeline. Churchill has a mean annual temperature of −7·2 C, with January being the coldest month (−27·5 C) and July the warmest (11·8 C). Only the months of June to September have mean temperatures above freezing. Annual precipitation is 411 mm, of which 43% is derived as snow during October to May. There are three major ecological zones that run roughly parallel to the coast: tundra, forest-tundra and open forest. Shallow lakes and ponds occur in all zones, but are most common in the tundra zone (occupying 32% of the landscape), less prevalent in the forest-tundra (24%) and least in the open forest (7%) (Lafleur *et al*., 1997). Lake depth rarely exceeds 3 m (Duguay and Lafleur, 2003). A summary of the general characteristics of the lakes sampled in the Churchill area is given in Table II.

Here, simulations were performed over a 45-year period, from 1955 to 1999, using meteorological data available from the Churchill Airport weather station operated by Environment Canada. A mean snow density of 235 kg m^{-3} was used in all simulations based on observations made during winter field campaigns in 1998 and 1999. The model was run using snow depth scenarios of 0% (snow-free) and 100% of the total measured at the weather station. Snow depths observed on lakes in this study area lie somewhere between these two extremes (Pivot *et al*., 2002).

Archived records of ice-on and ice-off dates for Farnworth Lake, located about 2 km south of the Churchill Airport runway, were used to validate model results over a 32-year period (1955–1986). These observations were extracted from the Canadian Ice Database (CID) (Lenormand *et al*., 2002). Satellite images and aerial photographs acquired during the break-up period were also used whenever available to validate ice-off dates for the 1990–91 to 1998–99 ice seasons. Landsat TM and SPOT (multispectral and panchromatic) browse images available from the Canada Centre for Remote Sensing were used for this purpose. These were preferred over AVHRR data because, although they provide a more frequent temporal coverage, the areal extent of many of the smaller lakes in the Churchill area is smaller than the pixel resolution of this sensor (1·1 km^2). The

Table II. Location and dimensions of Churchill lakes

Lake	Ecological zone	Latitude (N)	Longitude (W)	Area (km^2)	Depth (m)	
					Mean	Maximum
A	Tundra	58·75	93·82	0·8	0·8	1·5
58	Transition	58·72	93·78	2·0	2·4	3·2
Twin East	Open forest	58·62	93·80	1·3	1·1	1·8
Twin West	Open forest	58·62	93·82	0·9	1·8	2·2
Farnworth	Open forest	58·68	94·05	3·9	2·0	2·3

Copyright © 2003 John Wiley & Sons, Ltd.

temporal resolution of Landsat at the latitude of Churchill is 1 week, whereas that of SPOT (with its off-nadir pointing capabilities) is up to 2 days. Aerial photographs acquired on 22 June 1978, by the former Ministry of Mines and Natural Resources (now Natural Resources Canada), were also used to examine ice decay on lakes of various sizes in order to determine whether morphometry (depth, area) is an important determinant of ice-off dates. Also, simulated ice thickness was compared with measurements made during three field visits in winter 1997–98 (Duguay *et al*., 2002).

Poker Flat

The ponds investigated at Poker Flat are located in the boreal forest, 50 km northeast of Fairbanks, central Alaska. Situated within an 11 km radius of Poker Flat Research Range (65 07′N, 147 28′W, 200 m a.s.l.), the ponds occupy borrow pits resulting from road construction and typically have a maximum length <200 m, and mean depth of 2 m. The weather and climate at Poker Flat is similar to Fairbanks, where the mean annual temperature is −2·8 C, mean annual snowfall is 178 cm, and mean annual wind speed is 8·6 km h^{-1}. As a result, meteorological data from the Fairbanks NWS station were used for the simulations of winter 1999–2000.

A total of 10 ponds were visited during the winter period (Table III); four ponds were primary study sites and visited regularly, and six ponds were secondary sites that were visited occasionally in late winter. A subset of two to three ponds was visited every 2 weeks, and mean ice thickness, snow depth and snow density were calculated from all the data obtained on a particular day. Based on snow density measurements made on these ponds, independent runs were performed using snow densities of 155, 176 and 198 kg m^{-3}, representing the mean value plus or minus one standard deviation. Ice cores extracted from the primary ponds on 12 April 2000 were used to evaluate the ability of the model to simulate the proportion of snow-ice to total ice thickness. In contrast to Barrow and Churchill, no observations of ice-on or ice-off dates were made at Poker Flat.

RESULTS AND DISCUSSION

Ice-on and ice-off dates

The Canadian Lake Ice Model performed very well in matching the actual ice phenology over the 32-year period (1955–1986) in the Churchill area, as illustrated by the time-series of observed to simulated ice-on and ice-off dates from Farnworth Lake (Figure 4). Ice-on dates are simulated to within 2 days of observed values, and the mean absolute error in ice-off dates varies from 1 to 8 days depending on the snow cover scenario used in the simulations. The largest mean absolute error in ice-off dates is obtained when running

Table III. Pond names (all unofficial), number of visits and study site types at Poker Flat

Pond name	Number of visits	Site type
29·5	9	Primary
MST	10	Primary
LGP	9	Primary
SGP	8	Primary
31·6	3	Secondary
33·5	1	Secondary
34·0	2	Secondary
35·8	2	Secondary
36·6	2	Secondary

Copyright © 2003 John Wiley & Sons, Ltd.

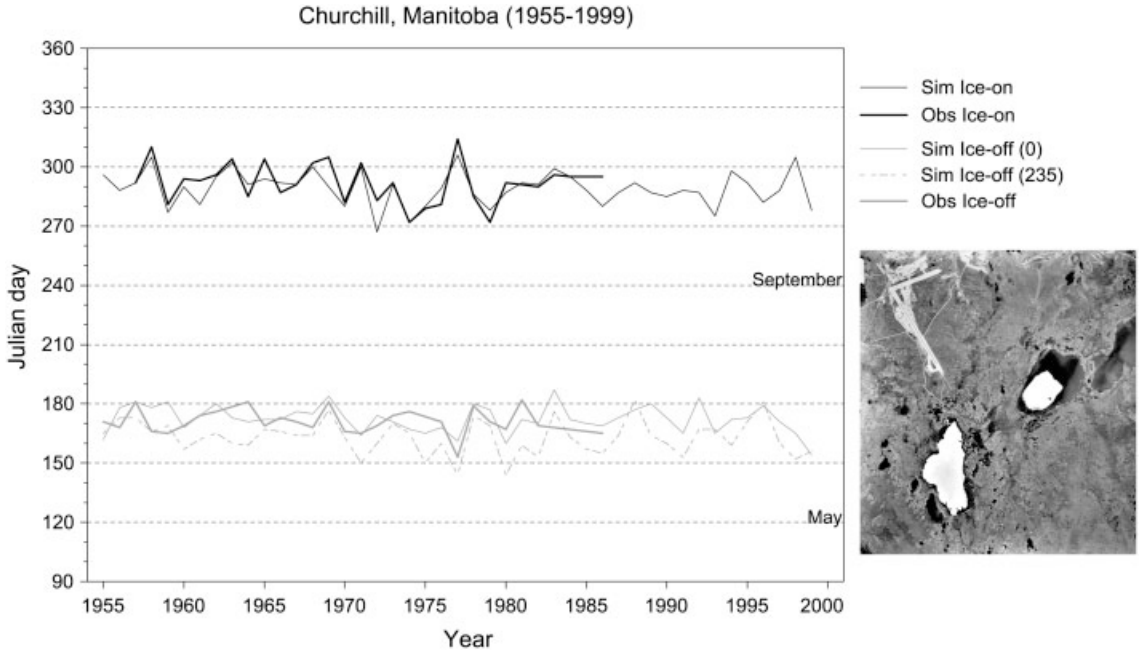

Figure 4. Simulated ice-on and ice-off dates between 1955 and 1998 compared with traditional *in situ* observations (1955–1986) at Farnworth Lake, Churchill, Manitoba. The two simulated ice-off time-series correspond to runs under snow-free conditions (0) and snow depths as measured at the Churchill Airport weather station with a mean winter snow density of 235 kg m^{-3}. Also shown is an aerial view of Farnworth Lake (long lake at bottom left, south of the airport runway) taken during the break-up period on 22 June 1978

the model with snow depths identical to those measured at the Churchill Airport weather station, indicating that the snow cover properties (e.g. depth and density) on Farnsworth Lake probably are different to those observed at the weather station owing to the redistribution of snow by winds. Unfortunately, no snow cover measurements were made on this lake to validate this argument with certainty.

Although the model simulations are in close agreement with the traditional lake-ice observations made at Farnworth Lake, airborne- and satellite-based observations provide a better, more objective, means of evaluating the ability of CLIMo to simulate lake-ice phenology spatially at the regional scale. During the 1977–78 ice season, for example, the model simulated ice-off dates between 23 and 29 June 1978. The suite of aerial photographs of Figure 5 show that some lakes were still ice-covered on the acquisition date of 22 June, although the field observer reported an ice-off date on 28 June for Farnworth Lake (see Figure 4). Table IV shows a comparison of model simulations and satellite-derived observations of ice-off dates for the Churchill study area. The satellite observations represent the estimated dates of when all lakes were completely free of ice. The satellite-derived dates are in close agreement (1–2 days) with the latest ice-off dates determined from model simulations for all years but spring 1994. We currently have no explanation for this discrepancy, other than greater snow accumulation and less snow redistribution by wind during that particular ice season. This means that the snow-free scenario (0%) was probably not encountered on the lakes in the study area, but if it did it was only for very short periods of time during winter 1993–94. A study by Boudreau and Rouse (1994) provides some support for this argument. They reported that snowfall was above normal both at the beginning of the freeze-up period (October) and the later part of winter (February and March) during that particular winter.

At Barrow, the simulated ice-off date for the 1991–92 ice season is also in close agreement with the date determined using ERS-1 SAR data. The latest ice-off date given by the model is 14 July 1992 (under the snow-free scenario), and a 15 July ice-off date has been derived from the analysis of ERS-1 images by Zhang

Copyright © 2003 John Wiley & Sons, Ltd.

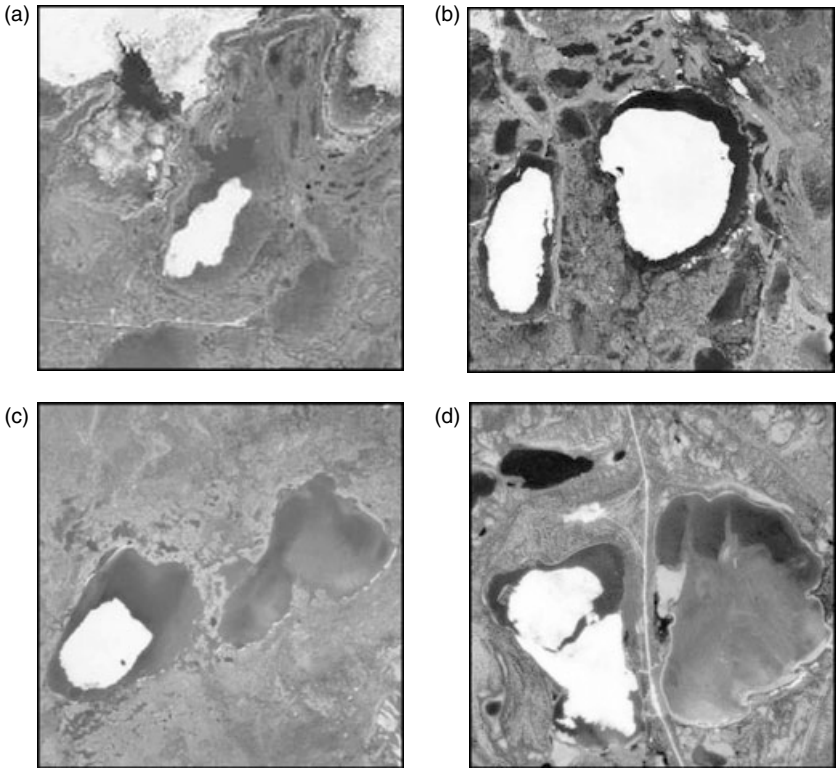

Figure 5. Aerial photographs (22 June 1978) of lakes in the Churchill study area showing the effect of lake depth on ice-off dates in (a) tundra zone (ice-covered lake A); forest-tundra transition zone, (b) Lake 58 (right) and Lindy Lake (left), and (c) Lake Stygge (east and west sections); and (d) open forest zone (Twin Lakes). See Table II for the size of some of these lakes

Table IV. Comparison between simulated ice-off dates and those derived from Landsat Thematic Mapper and SPOT (multispectral and panchromatic) images in the Churchill area

Ice Season	Simulated		Observed
	0% snow	100% snow	
1990–91	14 June	2 June	12 June
1991–92	1 July	15 June	N/A
1992–93	14 June	16 June	17 June
1993–94	21 June	8 June	11 June
1994–95	22 June	20 June	N/A
1995–96	27 June	29 June	27 June
1996–97	20 June	9 June	19 June
1997–98	14 June	1 June	15 June

and Jeffries (2000). The simulated ice-on date is 19 September 1991. According to Jeffries *et al.* (1994), autumn freeze-up at Barrow occurred between 11 and 20 September 1991, based on the analysis of ERS-1 images.

Returning to Figure 5 of the Churchill study area, one cannot help but notice the apparent role of lake morphometry on ice-off dates (see Table II for area and depth measurements). Based on our analysis of

Copyright © 2003 John Wiley & Sons, Ltd.

aerial photographs and satellite imagery, we find that lake depth, in particular, plays an important role during the spring break-up period. Through the analysis of late spring to early summer Landsat imagery, Sellmann *et al*. (1975a) also have noted the role of lake depth as a determinant of ice-off dates in the Barrow region. They observed that persistence of ice cover during the break-up period was associated with lake depth, the deeper lakes retaining their ice cover longest. The remote-sensing observations of Sellmann *et al*. (1975a) provide further evidence that the depth of these shallow lakes (at least those that are less than 4 m deep) is an important determinant of ice off-dates.

Although CLIMo provides generally good, consistent, simulation results for the shallow lakes examined herein, the role of lake morphometry (depth and area, which determine the water volume in a lake), especially during spring break-up, must be examined further. Mechanisms currently not considered in CLIMo, such as melt at the ice underside owing to seasonal variations of the heat flux from lake bottom sediments and lateral melt, once part of the lake is unfrozen (e.g. leads or open water areas at the margins of the decaying ice-cover), also must be investigated along with morphometry in order to determine their contribution to ice-melt. In its current form, CLIMo simulates a constant heat flux from the lake sediments. However, in reality, this heat flux is known to vary both temporally for a given lake and from one lake to another (e.g. Vavrus *et al*., 1996; Stefan and Fang, 1997).

Ice thickness and snow-ice formation

As shown in the previous section, snow cover plays a crucial role in controlling ice phenology. It is therefore important to represent as well as possible the spatial and temporal variation of snow cover to be able to simulate ice growth accurately. Ice-thickness evolution is especially sensitive to the timing and amount of snow accumulation early in the growth season. In general, simulation results of ice thickness obtained with CLIMo agree very well with measurements made on several lakes and ponds within the three study areas.

Results from the winter 1991–92 simulations at Barrow are shown in Figure 6. Maximum ice thickness simulated with the model varies between 227 and 174 cm, and differ as a function of snow depth, from no snow to 100% snow cover. Model results corresponding to the 19–29 April 1992 period can be compared with ice thickness measurements made in the field (Table V). Simulated ice thickness values range from 165 and 221 cm, whereas actual observations for the same period vary between 159 and 216 cm. This corresponds to a difference of only 5–6 cm during that particular ice season.

For the Churchill study area, most ice thickness measurements made on lakes in the three ecological zones during winter 1997–98 fall within the limits defined by the snow-free and 100% snow scenarios (Figure 7). The distribution of individual ice thickness observations on these lakes indicates that, indeed, snow accumulation differs between ecological zones, with the thinner ice covers observed on lakes in the open forest zone and the thicker ice covers in the tundra zone. This is consistent with the snow conditions apparent in photographs taken in the field during the same ice season (see Figure 3). Ice-melt from the bottom, as discussed earlier, or the parameterization of surface albedo in the model, are two possible factors that may explain the slight

Table V. Measured snow depth and ice thickness at lakes near Barrow, Alaska (19–29 April 1992) (after Jeffries *et al*., 1994)

Lake	Sampling date	Snow depth (cm)	Ice thickness (cm)
Emaiksoun site 1	20 April	0–5	210
Emaiksoun site 2	29 April	6	204
Emikpuk site 1	20 April	5	200·5
Emaikpuk site 2	28 April	2·5	216
Ikroavik site 1	19 April	3	194·5
Ikroavik site 2	19 April	6–8	159

Copyright © 2003 John Wiley & Sons, Ltd.

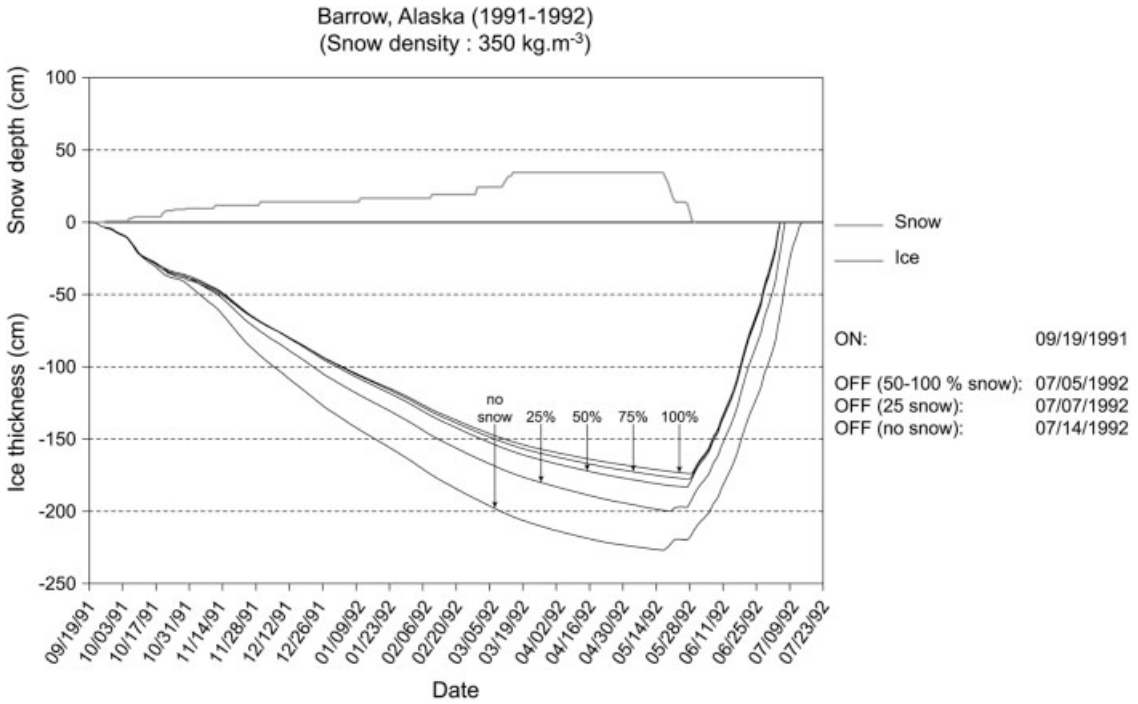

Figure 6. Simulated ice and snow thickness for lakes in the Barrow area, Alaska. A mean density of 350 kg m^{-3} was used for all runs based on field observations. Also shown are the simulated ice thickness for snow-free sites, and ice-on and ice-off dates. These can be compared with observed values reported in Table V

discrepancy between simulated and measured ice thickness at the forest site during the spring thaw of May 1998. A longer time-series of ice thickness observations would permit us to identify with greater confidence the factor(s) responsible for any systematic bias observable in model results.

In the Poker Flat study area, simulated ice thickness values obtained under the three different snow density scenarios also show little deviation from those measured in the field (Figure 8). The mean absolute error is only 2 cm for the entire winter period. The model slightly overestimates thickness at the beginning of the ice growth period, as shown by the deviation of field observations (dots) from the simulations (lines) in early to late November. Figure 8 also shows that the model captured slushing events, which did not occur on the lakes examined at Barrow and Churchill, and subsequent refreezing resulting in the formation of snow-ice layers. These events were also observed in the ice cores extracted from the primary ponds. Snow accumulation on the ponds, in this area of light winds, was sufficient to depress the ice surface below the hydrostatic level, thus saturating some fraction of the overlying snow cover. This slush then froze, thus producing the snow-ice layers observed in the ice cores.

However, as shown in Figure 9, CLIMo underestimated the total snow-ice thickness (12 April) by about 7 cm, when performing the simulation with the observed mean snow density of 176 kg m^{-3}. The mean snow-ice thickness obtained with the model is 28 cm, compared with 35 cm measured in the field. The simulated snow-ice thickness varies between 25 and 31 cm with the 155 and 198 kg m^{-3} scenarios, respectively. These results indicate that although the total ice (clear plus snow-ice) thickness simulated with the model closely match the observations, snow density changes from the moment of the first snow fall until spring thaw, including possible rainfall events (and further melt), need to be better accounted for. Also, during slushing events, the snow layer becomes soaked with water and some capillary suction probably exists so that the slush layer can actually be thicker than currently being simulated with CLIMo. The proper treatment of capillary

Copyright © 2003 John Wiley & Sons, Ltd.

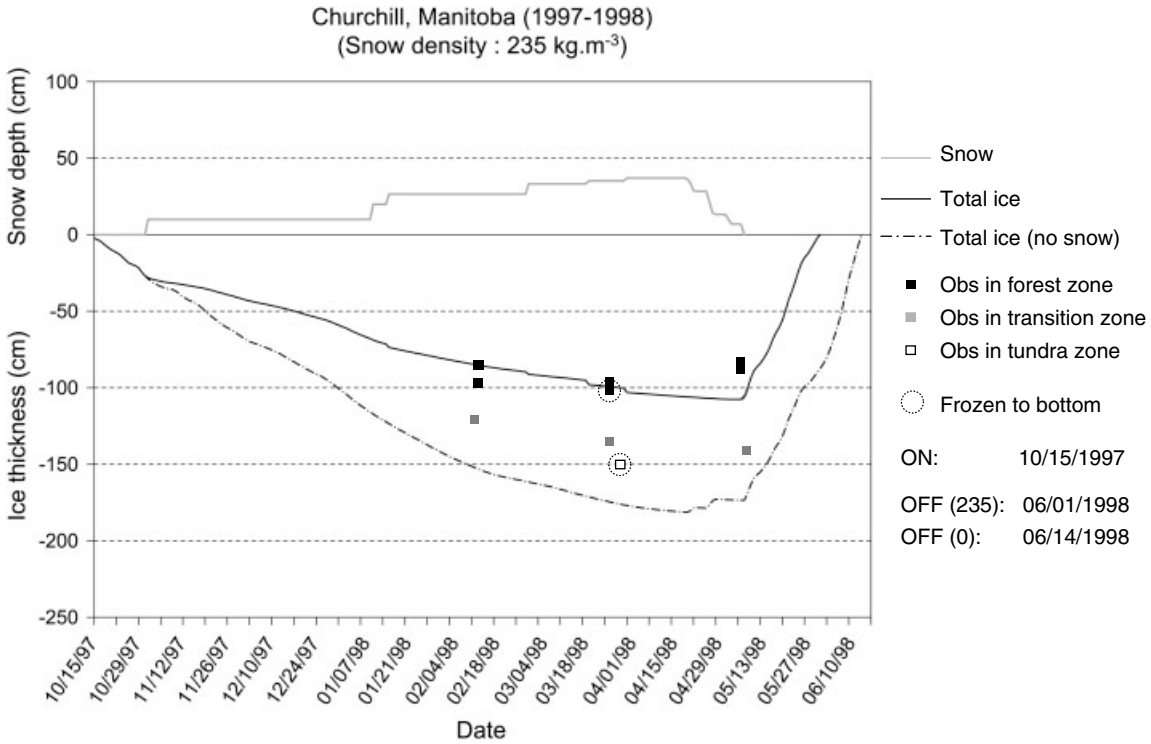

Figure 7. Simulated ice and snow thickness for lakes in the Churchill area, Manitoba. A mean density of 235 kg m^{-3} was used for all runs based on field observations. Also shown are the simulated ice thickness for snow-free sites, and ice-on and ice-off dates

suction in snow, however, is difficult because it requires information on snow grain and void size, and their distribution (e.g. Pfeffer *et al*., 1990; Saloranta, 2000).

CONCLUSIONS

A one-dimensional thermodynamic lake-ice model has been described and tested for simulating ice phenology on shallow lakes. Lake-ice models, such as the one presented in this paper, are a useful complement to observational (*in situ* and remote sensing) networks for studying the effect of climate on lake ice phenology. Models allow one to: (i) ascertain what climatic variables are reflected in freeze-up/break-up dates and hence how one might use freeze-up/break-up observations as an adjunct to more conventional (e.g. air temperature and precipitation) climate monitoring in data-sparse areas; (ii) understand sources of uncertainty or complications in interpreting freeze-up and break-up data (e.g. confounding effects of temperature and snowfall); (iii) estimate the magnitude of natural variability in freeze-up/break-up dates for use in climate change detection studies; and (iv) estimate potential impacts of changing climate on freeze-up/break-up dates as well as ice thickness and ice type (clear ice versus snow-ice).

The model generally performed quite well in reproducing ice-on and ice-off dates, and ice thickness on lakes in three contrasting high-latitude environments when compared with field and remote-sensing observations. The field observations made during several field campaigns in the study areas (e.g. Farnworth Lake, near Churchill) as well as the analysis of remote-sensing images enabled us to identify components of the model that may require more immediate attention. The most pronounced uncertainties in CLIMo

Copyright © 2003 John Wiley & Sons, Ltd.

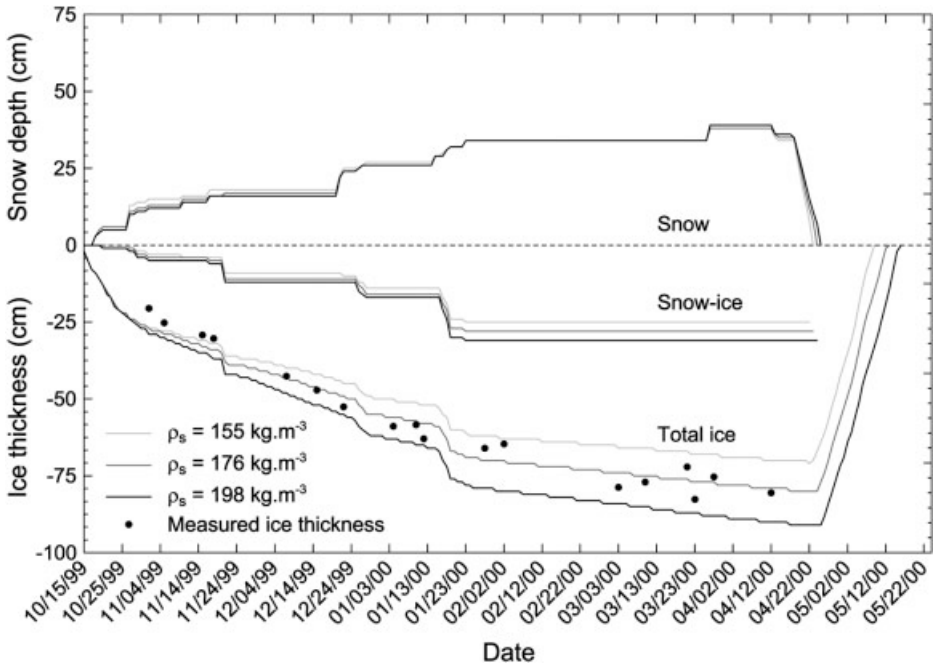

Figure 8. Simulated ice and snow thickness for Poker Flat ponds, Alaska. Mean snow densities of 176 kg m^{-3} ± 1 standard deviation were used for the simulations. Ice thickness measurements made *in situ* are also shown (dots)

were found to be related to the contribution of heat release from lake sediments and open-water areas to melt at the ice underside and lateral melt, and the handling of snow cover (e.g. lack of compaction and capillary suction during slushing events). The contribution of heat release from sediments has shown to be an important factor to consider when running the model on shallow lakes (e.g. Stefan and Fang, 1997).

The examination of aerial photographs, Landsat, SPOT and ERS-1 images on various dates allowed us to visualize spatially the effect of lake morphometry, in particular depth, on ice-off dates. This was made possible because of the synoptic, regional, view offered by remote-sensing products. The major advantage of remote-sensing data is that, unlike shore-based observations, they provide objective information on lake freeze-up/break-up over the entire lake surface.

This study also illustrated the key role of snow accumulation in determining the relative importance of lake-ice growth through bottom accretion and surface snow-ice growth mechanisms. The variable snow accumulation encountered in the three study areas was handled by adjusting snow depths observed at weather stations with measurements made on some lakes. Calculated mean winter snow density values for a limited number of field seasons were used for model runs. These averages most probably accounted for some of the discrepancies in model predictions. The use of more frequent snow depth and density measurements from snow courses, such as the bi-weekly observations available on CD from the Meteorological Service of Canada (MSC, 2000), could provide some improvements for nearby lake sites. Ultimately, relatively simple snow compaction equations (e.g. Anderson, 1976; Yen, 1981) or more sophisticated models such as SNTHERM (Jordan *et al.*, 1999) must be coupled or linked to CLIMo.

In the near future, we plan to carry out simulations on a larger number of lake sites of varied morphometry and to compare results with long historical records of ice and snow on-ice phenology across Canada. Some work is also envisaged on the effect of climate change, with a particular focus on snow and snow-ice

Copyright © 2003 John Wiley & Sons, Ltd.

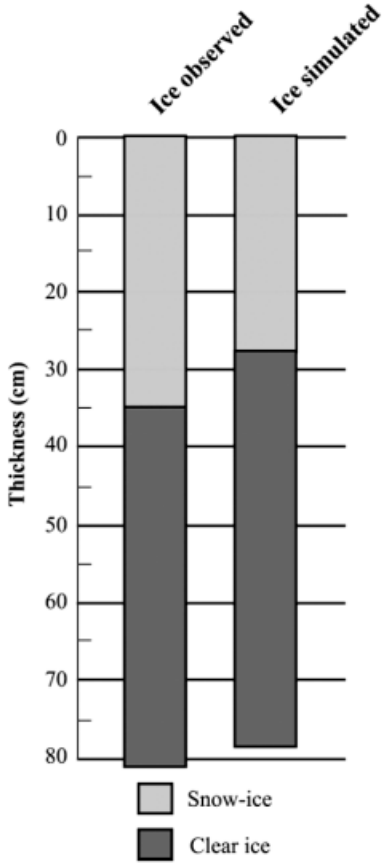

Figure 9. Simulated and observed mean ice thickness (clear ice and snow-ice) on 12 April 2000, from ponds at Poker Flat. A mean snow density of 176 kg m^{-3} was used for the simulation

formation in northern Canada and Alaska. The Canadian Lake Ice Model will be used to simulate these and examine the effect on the production of snow-ice and on the timing of break-up dates in particular. Snow-ice has optical and radiative properties distinctly different to clear ice (Liston and Hall, 1995). Being more reflective, hence allowing less light penetration, an increase in the proportion of snow-ice could have important consequences on the productivity of northern lakes. This is a plausible scenario given the increase in winter precipitation in the Arctic projected by recent global climate model runs (IPCC, 2001).

ACKNOWLEDGEMENTS

This work was conducted when C. Duguay was on sabbatical study leave as a Fulbright Scholar and Visiting Scientist with the International Arctic Research Center (IARC), University of Alaska Fairbanks. Support for this research was also provided by research grants from the Natural Sciences and Engineering Research Council of Canada (NSERC) and the Meteorological Service of Canada (MSC) to C. Duguay and W. Rouse, and IARC/CIFAR grants to C. Duguay, M. Jeffries and K. Morris, and NASA grants to M. Jeffries. The continued support of the Churchill Northern Studies Centre (CNSC) is greatly appreciated. This paper is a contribution to the CRYSYS project and Mackenzie GEWEX (MAGS-II) programme.

Copyright © 2003 John Wiley & Sons, Ltd.

NOTATION

Variables

$C_p(z, t)$	specific heat capacity (J kg^{-1} K^{-1})
$F_0(t)$	net downward heat flux absorbed at the surface (W m^{-2})
$F_{lat}(t)$	downward latent heat flux (W m^{-2})
$F_{lw}(t)$	downwelling longwave radiative energy flux (W m^{-2})
$F_{sw}(t)$	downwelling shortwave radiative energy flux (W m^{-2})
$F_{sens}(t)$	downward sensible heat flux (W m^{-2})
$h(t)$	total thickness of slab, ice plus snow (m)
$h_i(t)$	ice thickness (m)
$h_s(t)$	snow thickness (m)
$k(z, t)$	thermal conductivity (W m^{-1} K^{-1})
t	time (s)
$T(z, t)$	temperature within ice or snow (K)
$\hat{T}(z)$	the estimated temperature prior to solving (1) (K)
$T_{mix}(t)$	lake mixed layer temperature (K)
z	vertical coordinate, positive downward (m)
$\alpha(t)$	surface albedo
$\rho(z, t)$	density (kg m^{-3})

Parameters

C_{pi}	specific heat capacity of ice, $2{\cdot}062 \times 103$ J kg^{-1} K^{-1}
c_1	$2{\cdot}845 \times 10^{-6}$ W m^5 K^{-1} kg^{-2}
c_2	$2{\cdot}7 \times 10^{-4}$ W m^{-1} K^{-1}
c_3	233 K
c_4	1/5 K^{-1}
c_5	92·88 J kg^{-1} K^{-1}
c_6	7·364 J kg^{-1} K^{-2}
c_7	0·1 m
c_8	0·44 m$^{-0{\cdot}28}$
c_9	0·075 m^{-2}
d_{mix}	effective mixed layer depth (m)
h_{min}	minimum ice thickness below which open water is assumed, equal to 0·001 m
I_0	fraction of shortwave radiation flux that penetrates the surface, equal to 0·17 if snow depth $\leq$ 0·01 m, and equal to 0 if snow depth >0·1 m
k_{if}	conductivity of freshwater ice, equal to 2·034 W m^{-1} K^{-1}
L_{fi}	volumetric heat of fusion of freshwater ice, $3{\cdot}045 \times 10^8$ J m^{-3}
L_{fs}	volumetric heat of fusion of snow, $1{\cdot}097 \times 10^8$ J m^{-3}
T_f	freezing temperature of water, equal to 273·15 K
T_m	melting temperature at the surface, equal to 273·15 K
α	surface albedo
α_i	ice albedo
α_{ow}	albedo of open water, equal to 0·06
α_{mi}	albedo of melting ice, equal to 0·55
α_s	albedo of snow
Δt	time-step, equal to 86 400 s
ε	surface emissivity, equal to 0·99
K	bulk extinction coefficient for penetrating shortwave radiation, equal to 1·5 m^{-1}

Copyright © 2003 John Wiley & Sons, Ltd.

ρ_i	ice density, equal to 913 kg m^{-3}
ρ_s	snow density, equal to mean value observed in the field if snow temperature is below T_m and 450 kg m^{-3} if the average snow layer temperature is equal to T_m
ρ_w	water density, equal to 1000 kg m^{-3}
σ	Stefan–Boltzmann constant, $5{\cdot}67 \times 10^{-8}$ W m^{-2} K^{-4}

REFERENCES

Anderson EA. 1976. *A Point Energy and Mass Balance Model of a Snow Cover*. US National Oceanic and Atmospheric Administration NWS Technical Memorandum HYDRO-17: Silver-Spring, MD.

Blanken PD, Rouse WR, Culf AD, Spence C, Boudreau LD, Jasper JN, Kochtubajda B, Schertzer WM, Marsh P, Verseghy D. 2000. Eddy covariance measurements of evaporation from Great Slave Lake, Northwest Territories, Canada. *Water Resources Research* **36**: 1069–1077.

Boudreau DL, Rouse WR. 1994. *Algorithm testing of passive microwave monitoring of snow water equivalent in a tundra environment*. Final Report, Atmospheric Environment Service: Downsview, Ontario.

Duguay CR, Lafleur PM. 2003. Estimating depth and ice thickness of shallow subarctic lakes using spaceborne optical and SAR data. *International Journal of Remote Sensing*.

Duguay CR, Rouse WR, Lafleur PM, Boudreau DL, Crevier Y, Pultz TJ. 1999. Analysis of multi-temporal ERS-1 SAR data of subarctic tundra and forest in the northern Hudson Bay Lowland and implications for climate studies. *Canadian Journal of Remote Sensing* **25**: 21–33.

Duguay CR, Pultz TJ, Lafleur PM, Drai D. 2002. RADARSAT backscatter characteristics of ice growing on shallow sub-arctic lakes, Churchill, Manitoba, Canada. *Hydrological Processes* **16**: 1631–1644.

Ebert EE, Curry' JA. 1993. An intermediate one-dimensional thermodynamic sea ice model for investigating ice–atmosphere interactions. *Journal of Geophysical Research* **98**: 10 085–10 109.

Flato GM, Brown RD. 1996. Variability and climate sensitivity of landfast Arctic sea ice. *Journal of Geophysical Research* **101**(C10): 25 767–25 777.

Grosswald MG, Hughes TJ, Lasca NP. 1999. Oriented lake- and-ridge assemblages of the Arctic coastal plains: glacial landforms modified by thermokarst and solifluction. *Polar Record* **35**: 215–230.

Heron R, Woo M-K. 1994. Decay of a high arctic lake-ice cover: observations and modelling. *Journal of Glaciology* **40**: 283–292.

IPCC. 2001. *Climate Change 2001: The Scientific Basis*. Contribution of Working Group I to the Third Assessment Report of the Intergovernmental Panel on Climate Change (IPCC), Houghton JT, Ding Y, Griggs DJ, Noguer M, van der Linden PJ, Xiaosu D (eds). Cambridge University Press: Cambridge; 944 pp.

Jeffries MO, Morris K, Weeks WF, Wakabayashi H. 1994. Structural and stratigraphic features and ERS 1 synthetic aperture radar backscatter characteristics of ice growing on shallow lakes in NW Alaska, winter 1991–1992. *Journal of Geophysical Research* **99**: 22 459–22 471.

Jeffries MO, Morris K, Liston GE. 1996. A method to determine lake depth and water availability on the North Slope of Alaska with spaceborne imaging radar and numerical ice growth modelling. *Arctic* **49**: 367–374.

Jeffries MO, Zhang T, Frey K, Kozlenko N. 1999. Estimating late winter heat flow to the atmosphere from the lake–dominated Alaskan North Slope. *Journal of Glaciology* **45**: 315–324.

Jordan RE, Andreas EL, Makshtas AP. 1999. Heat budget of snow-covered sea ice at North Pole 4. *Journal of Geophysical Research* **104**(C4): 7785–7806.

Lafleur PM, Wurtele B, Duguay CR. 1997. Spatial and temporal variations in surface albedo of a subarctic landscape using surface-based measurements and remote sensing. *Arctic and Alpine Research* **29**: 261–269.

Lauriol B, Duguay CR, Riel A. 2002. Response of the Porcupine and Old Crow rivers in northern Yukon to Holocene climate change. *The Holocene* **12**: 27–34.

Lenormand F, Duguay CR, Gauthier R. 2002. Development of a historical ice database for the study of climate change in Canada. *Hydrological Processes* **16**: 3707–3722.

Liston GE, Hall DK. 1995. An energy-balance model of lake-ice evolution. *Journal of Glaciology* **41**: 373–382.

Livingstone DM. 1997. Break-up dates of alpine lakes as proxy data for local and regional mean surface air temperatures. *Climatic Change* **37**: 407–439.

Louis J-F. 1979. A parametric model of vertical eddy fluxes in the atmosphere. *Boundary Layer Meteorology* **17**: 187–202.

Maykut GA. 1982. Large-scale heat exchange and ice production in the central Arctic. *Journal of Geophysical Research* **87**: 7971–7984.

Maykut GA, Church PE. 1973. Radiation climate of Barrow, Alaska, 1962–66. *Journal of Applied Meteorology* **12**: 620–628.

Maykut GA, Untersteiner N. 1971. Some results from a time-dependent thermodynamic model of sea ice. *Journal of Geophysical Research* **76**: 1550–1575.

Mellor J. 1982. *Bathymetry of Alaskan Arctic lakes: a key to resource inventory with remote sensing methods*. PhD thesis, University of Alaska, Fairbanks.

Ménard P, Duguay CR, Flato GM, Rouse WR. 2002. Simulation of ice phenology on Great Slave Lake, Northwest Territories, Canada. *Hydrological Processes* **16**: 3691–3706.

Metcalfe JR, Goodison BE. 1993. Correction of Canadian winter precipitation data. Paper presented at the *Eighth Symposium on Meteorological Observations and Instrumentation*, 17–22 January, Anaheim, California, American Meteorological Society: Boston, MA.

MSC. 2000. *Canadian Snow Data CD-ROM*. CRYSYS Project, Climate Processes and Earth Observation Division, Meteorological Service of Canada: Downsview, Ontario.

Copyright © 2003 John Wiley & Sons, Ltd.

O'Neill D, Brown R, Agnew T, Burgess M, Cogley G, Demuth M, Duguay C, Flato G, Goodison B, Koerner R, Melling H, Prowse T, Ramsay B, Sharp M, Smith S, Walker A. 2001. *The Canadian GCOS Plan—Cryosphere*. Meteorological Service of Canada: 70 pp. Downsview, Ontario.

Pfeffer T, Illangasekare TH, Meier MF. 1990. Analysis and modeling of melt-water refreezing in dry snow. *Journal of Glaciology* **36**: 238–246.

Pivot F, Kergomard C, Duguay CR. 2002. On the use of passive microwave data to monitor spatial and temporal variations of snowcover near Churchill, Manitoba. *Annals of Glaciology* **34**: 58–64.

Saloranta TM. 2000. Modeling the evolution of snow, snow ice and ice in the Baltic Sea. *Tellus* **52A**: 93–108.

Schertzer WM. 1997. Freshwater lakes. In *The Surface Climates of Canada*, Bailey WB, Oke TR, Rouse WR (eds). McGill-Queens Press: Montreal and Kingston.

Schindler DW, Welch HE, Kalff J, Brunskill GJ, Kritsch N. 1974. Physical and chemical limnology of Char Lake, Cornwallis Island (75 N). *Journal of the Fisheries Research Board, Canada* **31**: 585–607.

Sellmann PV, Brown J, Lewellen RI, McKim H, Merry C. 1975a. *The Classification and Geomorphic Implications of Thaw Lakes on the Arctic Coastal Plain, Alaska*. Research Report 344, Cold Regions Research Engineering Laboratory: Hanover, NH.

Sellmann PV, Weeks WF, Campbell WJ. 1975b. *Use of Sidelooking Airborne Radar to Determine Lake Depth on the Alaskan North Slope*. Special Report 230, Cold Regions Research Engineering Laboratory: Hanover, NH.

Shine KP. 1984. Parameterization of the shortwave flux over high albedo surfaces as a function of cloud thickness and surface albedo. *Quarterly Journal of the Royal Meteorological Society* **110**: 747–764.

Stefan HG, Fang X. 1997. Simulated climate change effects on ice and snow covers on lakes in a temperate region. *Cold Regions Science and Technology* **25**: 137–152.

Stewart RB, Rouse WR. 1977. Substantiation of the Priestley and Taylor parameter = 1·26 for potential evaporation in high latitudes. *Journal of Applied Meteorology* **16**: 649–650.

Vavrus SJ, Wynne RH, Foley JA. 1996. Measuring the sensitivity of southern Wisconsin lake ice to climate variations and lake depth using a numerical model. *Limnology and Oceanography* **41**: 822–831.

Yen Y. 1981. *Review of Thermal Properties of Snow and Sea Ice*. Report 81-10, US Army Cold Regions Research Engineering Laboratory: Hanover, NH.

Zhang T, Jeffries MO. 2000. Modeling inter-decadal variations of lake ice thickness and sensitivity to climate change on northernmost Alaska. *Annals of Glaciology* **31**: 339–347.

Copyright © 2003 John Wiley & Sons, Ltd.